

BeppoSAX Observations of 1-Jy BL Lacertae Objects. I.

Paolo Padovani^{1,2,3,*}, Luigi Costamante⁴, Paolo Giommi⁵, Gabriele Ghisellini⁶,
 Andrea Comastri⁷, Anna Wolter⁸, Laura Maraschi⁸, Gianpiero Tagliaferri⁶,
 C. Megan Urry¹

¹ *Space Telescope Science Institute, 3700 San Martin Drive, Baltimore MD. 21218, USA*

² *Affiliated to the Astrophysics Division, Space Science Department, European Space Agency*

³ *On leave from Dipartimento di Fisica, II Università di Roma “Tor Vergata”, Via della Ricerca Scientifica 1, I-00133 Roma, Italy*

⁴ *Università degli Studi di Milano, Milano, Italy*

⁵ *BeppoSAX Science Data Center, ASI, Via Corcolle 19, I-00131 Roma, Italy*

⁶ *Osservatorio Astronomico di Brera, Via Bianchi 46, I-23807 Merate, Italy*

⁷ *Osservatorio Astronomico di Bologna, Via Ranzani 1, I-40127 Bologna, Italy*

⁸ *Osservatorio Astronomico di Brera, Via Brera 28, I-20121 Milano, Italy*

Accepted , Received

ABSTRACT

We present new *BeppoSAX* observations of seven BL Lacertae objects selected from the 1 Jy sample plus one additional source. The collected data cover the energy range 0.1 – 10 keV (observer’s frame), reaching ~ 50 keV for one source (BL Lac). All sources characterized by a peak in their multifrequency spectra at infrared/optical energies (i.e., of the LBL type) display a relatively flat ($\alpha_x \sim 0.9$) X-ray spectrum, which we interpret as inverse Compton emission. Four objects (2/3 of the LBL) show some evidence for a low-energy steepening which is likely due to the synchrotron tail merging into the inverse Compton component around $\sim 1 - 3$ keV. If this were generally the case with LBL, it would explain why the 0.1 – 2.4 keV ROSAT spectra of our sources are systematically steeper than the *BeppoSAX* ones ($\Delta\alpha_x \sim 0.5$). The broad-band spectral energy distributions fully confirm this picture and a synchrotron inverse Compton model allows us to derive the physical parameters (intrinsic power, magnetic field, etc.) of our sources. Combining our results with those obtained by *BeppoSAX* on BL Lacs covering a wide range of synchrotron peak frequency, ν_{peak} , we confirm and clarify the dependence of the X-ray spectral index on ν_{peak} originally found in ROSAT data.

Key words: galaxies: active – BL Lacertae objects: general – X-rays: galaxies

1 INTRODUCTION

BL Lacertae objects constitute one of the most extreme classes of active galactic nuclei (AGN), distinguished by their high luminosity, rapid variability, high ($> 3\%$) optical polarization, radio core-dominance, apparent superluminal speeds, and almost complete lack of emission lines (e.g., Kollgaard 1994; Urry & Padovani 1995). The broad-band emission in these objects, which extends from the radio to the gamma-ray band, appears to be dominated by non-thermal processes from the heart of the AGN, undiluted by the thermal emission present in other AGN. Therefore, BL Lacs represent the ideal class to study to further our understanding of non-thermal emission in AGN.

Synchrotron emission combined with inverse Compton scattering is generally thought to be the mechanism responsible for the production of radiation over such a wide energy range (e.g., Ghisellini et al. 1998). The synchrotron peak frequency, ν_{peak} , ranges across several orders of magnitude, going from the far-infrared to the hard X-ray band (e.g., Sambruna et al. 1996; Fossati et al. 1998). Sources at the extremes of this wide distribution are referred to as low-energy peaked (LBL) and high-energy peaked (HBL) BL Lacs, respectively (Giommi & Padovani 1994; Padovani & Giommi 1995). Radio-selected samples include mostly objects of the LBL type, while X-ray selected samples are mostly made up of HBL.

This scenario gives clear and strong predictions on the X-ray spectra for the two classes. In the relatively narrow ROSAT band differences between the two classes became

* Email: padovani@stsci.edu

apparent only when very large BL Lac samples ($\sim 50\%$ of the then known objects) were considered (Padovani & Giommi 1996; Lamer, Brunner & Staubert 1996). The *BeppoSAX* satellite (Boella et al. 1997a), with its broad-band X-ray (0.1 – 200 keV) spectral capabilities, is particularly well suited for a detailed analysis of the individual X-ray spectra of these sources.

In this paper we present *BeppoSAX* observations of eight BL Lacs, including six LBL and two HBL. The sample is well defined (in particular, it is not a compilation of known hard X-ray sources) being extracted, apart from one source, from the radio-selected 1-Jy sample, for which a wealth of information at many wavelengths is available.

In § 2 we present our sample, § 3 discusses the observations and the data analysis, while § 4 describes the results of our spectral fits to the *BeppoSAX* data. § 5 deals with the ROSAT data for our sources, while § 6 presents the spectral energy distributions and synchrotron-inverse Compton fits to the data, and § 7 deals with the dependence of the X-ray spectral index on synchrotron peak frequency. Finally, § 8 discusses our conclusions. Throughout this paper spectral indices are written $S_\nu \propto \nu^{-\alpha}$.

2 THE SAMPLE

The 1 Jy sample of BL Lacs is presently the only sizeable, complete sample of radio bright BL Lacs. It includes 34 objects with radio flux > 1 Jy at 5 GHz (Stickel et al. 1991). All 1 Jy BL Lacs have been studied in detail in the radio and optical bands; all objects have also soft X-ray data, primarily from ROSAT.

We selected for *BeppoSAX* observations all 1 Jy BL Lacs with 0.1 – 10 keV X-ray flux larger than 2×10^{-12} erg cm $^{-2}$ s $^{-1}$ (estimated from an extrapolation of the single power-law fits derived for these objects from ROSAT data; Urry et al. 1996). This included twenty 1 Jy BL Lacs (or $\sim 60\%$ of the sample). Some of these sources have been included in other *BeppoSAX* programs (e.g., MKN 501: Pian et al. 1998; S5 0716+714: Giommi et al. 1999). We present here the results obtained for the 7 objects observed in Cycle 1 plus B2 0912+29, which was included in a program aimed at studying “intermediate” BL Lacs. All sources apart from PKS 2005–489 and B2 0912+29 are LBL. The object list and basic characteristics are given in Table 1, which presents the source name, type, position, redshift, R magnitude, 5 GHz radio flux, and Galactic N_H .

3 OBSERVATIONS AND DATA ANALYSIS

A complete description of the *BeppoSAX* mission is given by Boella et al. (1997a). The relevant instruments for our observations are the coaligned Narrow Field Instruments (NFI), which include one Low Energy Concentrator Spectrometer (LECS; Parmar et al. 1997) sensitive in the 0.1 – 10 keV band; three identical Medium Energy Concentrator Spectrometers (MECS; Boella et al. 1997b), covering the 1.5 – 10 keV band; and the Phoswich Detector System (PDS; Frontera et al. 1997), coaligned with the LECS and the MECS. The PDS instrument is made up of four units, and was operated in collimator rocking mode, with a pair of units pointing

at the source and the other pair pointing at the background, the two pairs switching on and off source every 96 seconds. The net source spectra have been obtained by subtracting the ‘off’ to the ‘on’ counts. A journal of the observations is given in Table 2.

The data analysis was based on the linearized, cleaned event files obtained from the *BeppoSAX* Science Data Center (SDC) on-line archive (Giommi & Fiore 1997). The data from the three MECS instruments were merged in one single event file by the SDC, based on sky coordinates. The event file was then screened with a time filter given by SDC to exclude those intervals related to events without attitude solution (i.e., conversion from detector to sky coordinates; see Handbook for NFI Spectral Analysis, F. Fiore et al., 1999). This was done to avoid an artificial decrease in the flux. As recommended by the SDC, the channels 1–10 and above 4 keV for the LECS and 0–36 and 220–256 for the MECS were excluded from the spectral analysis, due to residual calibration uncertainties. Except for PKS 1519–273, where an extraction radius of 4 arcmin was used for the LECS (see below), spectra and lightcurves have been extracted using the standard extraction radii of 8 and 4 arcmin, for the LECS and MECS respectively.

The spectral analysis was performed using the matrices and blank-sky background files released in November 1998 by the SDC. For the LECS, we were careful to choose the blank-sky file extracted in the same coordinate frame as the source file. This is necessary to avoid an error in the background subtraction that arises when using source and background files extracted in coordinate frames of different pixel size (in this case, raw and detector or sky coordinates). Raw pixels, in fact, have a size of 14 arcsec, while detector and sky pixels have a size of 8 arcsec. Therefore, an equal extraction region of 8 arcmin, for example, is obtained with a different number of pixels. In this situation, however, the spectral files extracted in the two cases have different values of the keyword used in the analysis software to rescale the background to the source extraction area. The two files, in short, appear to have been extracted with different areas (the difference is $\sim 35\%$), and the background in such case would be wrongly rescaled accordingly.

Because of the importance of the band below 1 keV to assess the presence of extra absorption or soft excess (indicative of a double power-law spectrum), we have also checked the LECS data for differences in the cosmic background between local and blank-sky field observations, comparing spectra extracted from the same areas on the detector (namely, two circular regions outside the 10’ radius central region, located at the opposite corners with respect to the two on-board radioactive calibration sources). No relevant differences were found, except in the BL Lac and PKS 1519–273 observations.

For BL Lac, the blank-sky background up to 0.5–0.6 keV is higher than that during our observation, causing a low level of counts in the source spectrum. The signal-to-noise ratio (S/N) at low energy, however, is very low, due to the high galactic absorption ($\sim 2 - 3.6 \times 10^{21}$ cm $^{-2}$, see Tab. 1), and no detection is expected below 0.3 – 0.4 keV. In a conservative approach, we have therefore limited the spectral analysis to energies above 0.5 keV. However, we also checked the results down to 0.1 keV using a different background file, obtained multiplying the blank-sky field at

Table 1. Sample Properties

Name	Type	RA(J2000)	Dec(J2000)	z	R_{mag}^a	$F_{5\text{GHz}}$ Jy	Galactic N_{H} 10^{20} cm^{-2}
PKS 0048–097	LBL	00 50 41.3	−09 29 06	>0.2	16.5	2.0	3.85
OJ 287	LBL	08 54 49.0	+20 06 32	0.306	15.0	2.6	2.75 ^b
B2 0912+29	HBL	09 15 52.3	+29 33 21	...	15.8 ^c	0.2	2.11
PKS 1144–379	LBL	11 47 01.4	−38 12 10	1.048	16.5	1.6	7.64
PKS 1519–273	LBL	15 22 37.7	−27 30 10	>0.2	18.5	2.4	8.66
4C 56.27	LBL	18 24 07.2	+56 51 00	0.664	18.5	1.7	4.16
PKS 2005–489	HBL	20 09 25.4	−48 49 55	0.071	13.5	1.2	5.08
BL Lac	LBL	22 02 43.2	+42 16 40	0.069	14.0	4.8	20.15 ^b , total 36 ^d

^a mean R magnitude from Heidt & Wagner (1996)

^b from Elvis et al. 1989

^c V magnitude from Tapia et al. (1976)

^d including a molecular cloud along the line of sight (see Sambruna et al. 1999)

Table 2. BeppoSAX Journal of observations

Name	LECS exp. (s)	LECS count rate ^a (cts/s)	MECS exp. (s)	MECS count rate ^a (cts/s)	PDS exp. (s)	PDS count rate ^a (cts/s)	Observing date
PKS 0048–097	4602	0.020 ± 0.006	9810	0.023 ± 0.002	1997 Dec 19
OJ 287	5105	0.018 ± 0.006	10707	0.032 ± 0.002	4511	0.128 ± 0.094	1997 Nov 24
B2 0912+29	9195	0.054 ± 0.004	23832	0.048 ± 0.002	1997 Nov 14-15
PKS 1144–379	10649	0.010 ± 0.003	22754	0.019 ± 0.001	1997 Jan 10-11
PKS 1519–273	9266	0.009 ± 0.003	26906	0.009 ± 0.001	1998 Feb 1
4C 56.27	4104	0.014 ± 0.007	13382	0.015 ± 0.001	1997 Oct 11
PKS 2005–489	9853	1.371 ± 0.012	1996 Sep 29-30
BL Lac	12260	0.094 ± 0.003	13750	0.150 ± 0.003	8278	0.191 ± 0.094	1997 Nov 8

^a net count rate full band

the source position by the ratio of the local to blank field backgrounds extracted in the two areas far from the source. This should give an estimate of the local background at the source position. No significant differences or trends between the two cases were found.

For PKS 1519–273, the local background presents an anomalously high flux between ~ 0.7 and 1 keV. This feature is also present in the backgrounds extracted from the two circular regions independently, so it is unlikely that its cause could be a very faint serendipitous source. This problem becomes more evident with larger extraction radii, due to the very low flux of the source. To minimize this effect and increase the S/N, an extraction radius of 4 arcmin was used. Minor differences were found for PKS 1144–379: the local background was uniformly higher by $\sim 20\%$, so the blank field background was rescaled accordingly, as suggested by the SDC (see Handbook for NFI spectral Analysis).

3.1 Time analysis

Using the software package XRONOS we looked for time variability in every observation, binning the data in intervals from 500 to 4000 s, with null results except for PKS 1144–379. In this case, there might be an indication of variability, as the lightcurves present a “wave-like” shape, in particular on time-scales ~ 5 hours. The resulting χ^2 value is consistent with no variability at the $\sim 3\%$ level so this result is not compelling, but the same pattern is present in every single MECS detector, within the uncertainties. This level remains roughly constant across different binnings, given

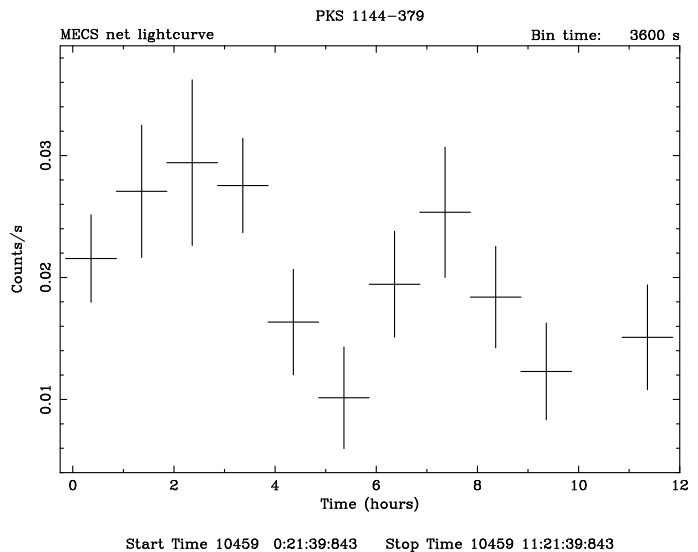
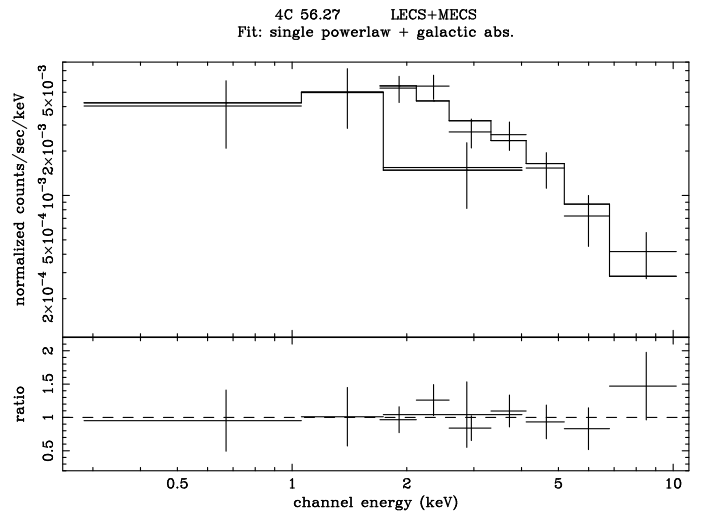
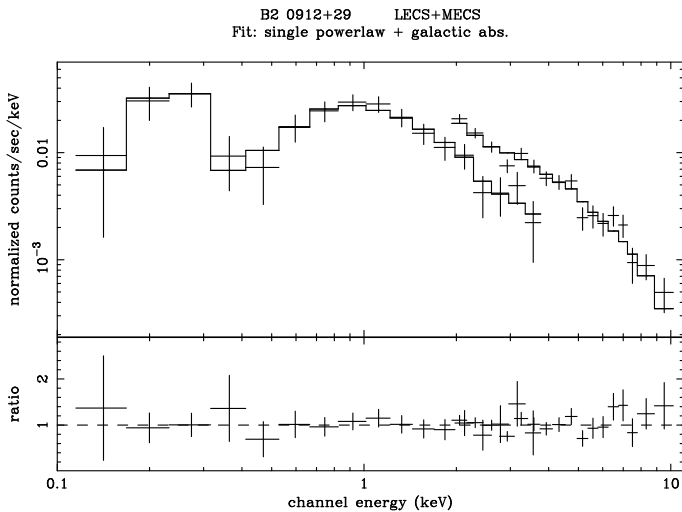
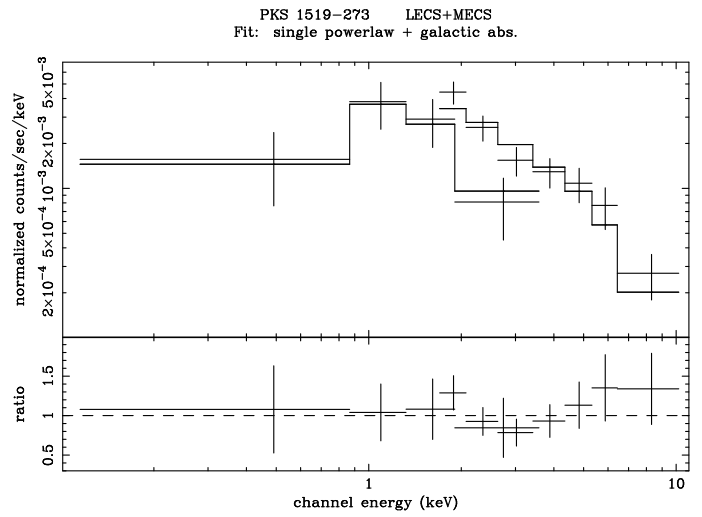
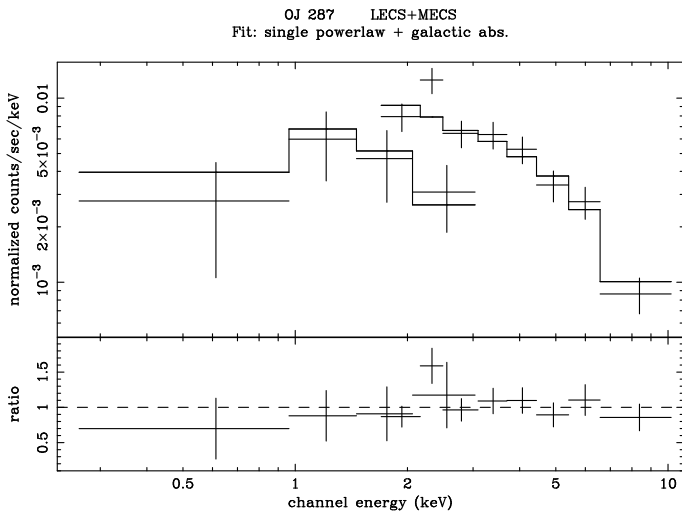
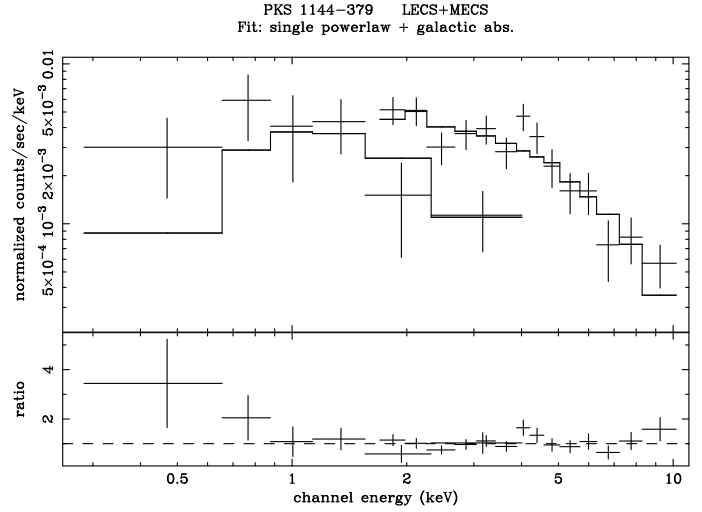
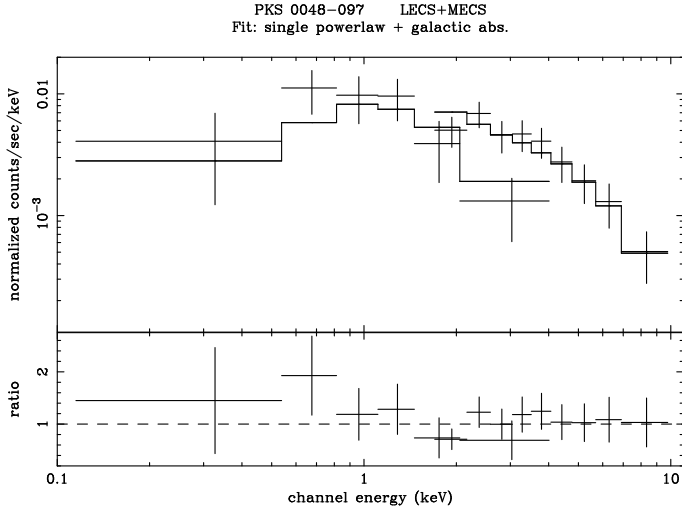


Figure 1. The net source lightcurve of the three MECS units for PKS 1144–379. The apparent variability is significant at the 97% level.

sufficient statistics (i.e., with time bins $\gtrsim 1200$ s). Also considering the whole sample, the significance is “borderline”: a spurious variability of this level is expected, on average, every ~ 33 observations, in the hypothesis of a parent population of constant sources. In our case this translates to 0.24 times every 8 sources. The LECS light curve is much less sampled and consistent with no variability at the $\sim 17\%$



level, although similar in shape to the MECS one. An inspection of the local background lightcurve showed no significant variation. Fig. 1 shows the net source lightcurve of the three MECS units merged together. If the variations are real, the source varied up to a factor ~ 3 in 4 hours.

4 SPECTRAL FITS

The spectral analysis was performed with the XSPEC 10.0 package. Using the program GRPPHA, the spectra were rebinned with more than 20 counts in every new bin and using the rebinning files provided by the SDC. Various checks using different rebinning strategies have shown that our results are independent of the adopted rebinning within the

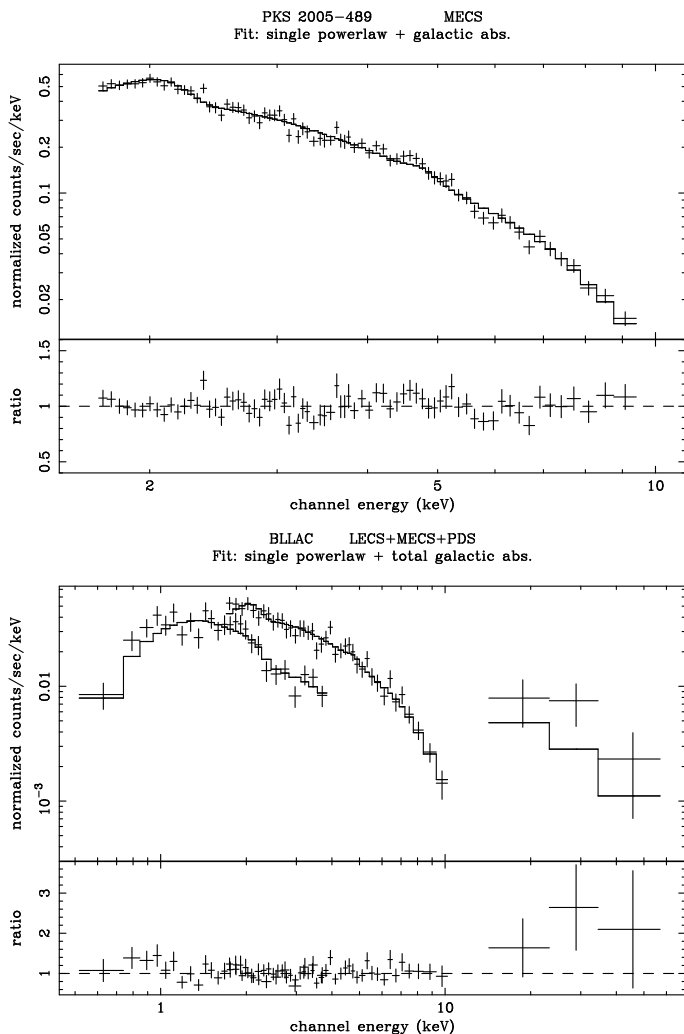


Figure 2. *BeppoSAX* data and fitted spectra for our sources, and ratio of data to fit. Data are from the LECS and MECS instruments, apart from PKS 2005–489, which only has MECS data, and BL Lac, which has also a PDS detection. The data are fitted with a single power-law model with Galactic absorption.

uncertainties. The data were analyzed applying the Gehrels statistical weight (Gehrels 1986), in case the resulting net counts were below 20 (typically 12–15 in the low energy band of LECS). The LECS/MECS normalization factor was left free to vary in the range 0.65–1.0, as suggested by SDC (see Handbook for NFI spectral Analysis). The X-ray spectra of our sources are shown in Fig. 2.

4.1 Power-law Fits

At first, we fitted the combined LECS and MECS data with a single power-law model with Galactic and free absorption. The absorbing column was parameterized in terms of N_{H} , the HI column density, with heavier elements fixed at solar abundances and cross sections taken from Morrison and McCammon (1983). The Galactic value was derived from the `nh` program at HEASARC (based on Dickey & Lockman 1990), when more accurate estimates were not available (see Table 1). The Galactic N_{H} value for BL Lac was fixed at two values: that from Elvis, Lockman & Wilkes (1989),

based on dedicated 21 cm observations, and the sum of this value and that inferred from millimeter observations, which include the contribution from molecular hydrogen (Lucas & Liszt 1993). The N_{H} parameter was also set free to vary for all sources (apart from PKS 2005–489, which has no LECS data) to check for intrinsic absorption and/or indications of a “soft-excess.”

Our results are presented in Table 3, which gives the name of the source in column (1), N_{H} in column (2), the energy index α_{x} in column (3), the 1 keV flux in μJy in column (4), the unabsorbed 2–10 keV and 0.1–2.4 keV fluxes in columns (5)–(6), the LECS/MECS normalization in column (7), the reduced chi-squared and number of degrees of freedom, $\chi^2_{\nu}/(\text{dof})$ in column (8), and the F-test probability that the decrease in χ^2 due to the addition of a new parameter (free N_{H}) is significant in column (9). The errors quoted on the fit parameters are the 90% uncertainties for one and two interesting parameters, for Galactic and free N_{H} respectively. The errors on the 1 keV flux reflect the statistical errors only and not the model uncertainties.

Two results are immediately apparent from Table 3. First, the fitted N_{H} values agree with the Galactic ones for most sources (within the rather large errors); this is confirmed by an *F*-test which shows that the addition of N_{H} as a free parameter does not result in a significant improvement in the χ^2 values (column 9 of Table 3), with the exception of BL Lac (*F*-test done for larger N_{H} value). Second, the fitted energy indices are relatively flat, $\alpha_{\text{x}} \lesssim 1$ within the errors for all but two sources. The mean value is $\langle \alpha_{\text{x}} \rangle = 0.98 \pm 0.10$ and the weighted mean is $\langle \alpha_{\text{x}} \rangle = 1.26 \pm 0.03$. This latter value is clearly dominated by PKS 2005–489, an HBL with a very well determined slope. Excluding this source and the other HBL, B2 0912+29, we derive a mean value $\langle \alpha_{\text{x}} \rangle = 0.87 \pm 0.09$ and a weighted mean $\langle \alpha_{\text{x}} \rangle = 0.83 \pm 0.09$.

Some of our sources appear to show a low-energy excess, as illustrated by the fact that the best fit N_{H} in Table 3 is below the Galactic value for four sources, namely PKS 0048–097, PKS 1144–379, PKS 1519–273, and BL Lac. We then fitted a broken power-law model to these data. Although this resulted in a better fit, an *F*-test shows that the improvement is more suggestive than significant, with probabilities ranging from 86–88% for PKS 0048–097 and PKS 1144–379, to $\sim 93\%$ for PKS 1519–273 and BL Lac. The best-fit spectra, however, all point in the same direction: a flatter component emerging at higher energies. In fact, they are all obviously concave with quite a large spectral change, with $\langle \alpha_{\text{S}} - \alpha_{\text{H}} \rangle = 0.8 \pm 0.1$, and energy breaks around $E \sim 1 - 3$ keV. The hard X-ray spectral index is $\langle \alpha_{\text{H}} \rangle = 0.6 \pm 0.1$, while $\langle \alpha_{\text{S}} \rangle = 1.5 \pm 0.1$. Some evidence for concave spectra comes also from the shape of the ratio of the data to the single power-law fits, shown in Fig. 2. We note that by adding up the χ^2 values for the four sources, an *F*-test shows that the improvement in the fit provided by a double power-law model *for the four sources together* is significant at the $\sim 96\%$ level.

4.2 The PDS Detections

Two sources were detected also by the PDS instrument: BL Lac and OJ 287. Due to the low statistics, the spectra have been heavily rebinned, resulting in three and one points for BL Lac and OJ 287 respectively, in the detection range.

Table 3. Single power-law fits, LECS + MECS

Name	N_H 10^{20} cm^{-2}	α_x	$F_{1\text{keV}}$ μJy	$F_{[2-10]}$ $\text{erg cm}^{-2} \text{ s}^{-1}$	$F_{[0.1-2.4]}$ $\text{erg cm}^{-2} \text{ s}^{-1}$	Norm (LeCS/MeCS)	χ^2_ν/dof	F-test, notes fixed-free N_H
PKS 0048–097	3.85 fixed	$0.9^{+0.4}_{-0.4}$	$0.3^{+0.2}_{-0.1}$	1.45e-12	2.37e-12	0.82	0.58/12	
	2.0(< 18)	$0.9^{+0.5}_{-0.5}$	$0.3^{+0.2}_{-0.1}$	1.48e-12	2.11e-12	0.81	0.59/11	63%
OJ 287	2.75 fixed	$0.6^{+0.2}_{-0.2}$	$0.3^{+0.1}_{-0.1}$	2.46e-12	2.05e-12	0.66	1.00/9	
	21(< 163)	$0.7^{+0.6}_{-0.4}$	$0.4^{+0.4}_{-0.1}$	2.47e-12	2.65e-12	0.66	0.97/8	70%
B2 0912+29	2.11 fixed	$1.3^{+0.1}_{-0.1}$	$1.1^{+0.1}_{-0.1}$	2.86e-12	1.01e-11	0.74	0.76/38	
	$2.8^{+1.6}_{-1.1}$	$1.3^{+0.2}_{-0.2}$	$1.2^{+0.2}_{-0.2}$	2.80e-12	1.17e-11	0.73	0.74/37	86%
PKS 1144–379	7.64 fixed	$0.6^{+0.3}_{-0.2}$	$0.14^{+0.06}_{-0.04}$	1.00e-12	0.89e-12	0.91	1.03/17	
	0.0(< 21)	$0.6^{+0.3}_{-0.3}$	$0.14^{+0.05}_{-0.03}$	0.99e-12	0.87e-12	0.86	0.98/16	82%
PKS 1519–273	8.66 fixed	$1.1^{+0.4}_{-0.4}$	$0.2^{+0.1}_{-0.1}$	0.62e-12	1.51e-12	0.77	0.67/8	
	5.2(< 44)	$1.0^{+0.6}_{-0.5}$	$0.2^{+0.1}_{-0.1}$	0.63e-12	1.32e-12	0.76	0.74/7	36%
4C 56.27	4.16 fixed	$1.1^{+0.3}_{-0.4}$	$0.3^{+0.1}_{-0.1}$	0.98e-12	2.35e-12	0.71	0.49/7	
	5.7(< 75)	$1.1^{+0.7}_{-0.5}$	$0.3^{+0.2}_{-0.1}$	0.98e-12	2.41e-12	0.72	0.57/6	10%
PKS 2005–489	5.08 fixed	$1.33^{+0.04}_{-0.04}$	$25.4^{+1.1}_{-1.1}$	6.09e-11	2.60e-10	—	1.04/73	—
BL Lac	20.15 fixed	$0.83^{+0.08}_{-0.08}$	$2.2^{+0.2}_{-0.3}$	1.12e-11	1.54e-11	0.72	0.92/63	21 cm maps
	36.0 fixed	$0.96^{+0.08}_{-0.08}$	$2.7^{+0.3}_{-0.3}$	1.11e-11	2.03e-11	0.75	0.94/63	H atom. + molec.
	27^{+10}_{-8}	$0.89^{+0.13}_{-0.13}$	$2.4^{+0.4}_{-0.3}$	1.12e-11	1.74e-11	0.73	0.89/62	96%
	36.0 fixed	$0.95^{+0.08}_{-0.08}$	$2.7^{+0.3}_{-0.3}$	1.12e-11	1.97e-11	0.75	0.96/66	including PDS ^a
	26^{+10}_{-8}	$0.87^{+0.13}_{-0.13}$	$2.4^{+0.3}_{-0.3}$	1.12e-11	1.67e-11	0.73	0.90/65	including PDS ^a

^a PDS maximum detection 3.8σ between 13 and 35 keV

Note: unless otherwise indicated, the errors are at 90% confidence level for one (with fixed N_H) and two parameters of interest.

The significance level of the detection, obtained grouping the channels, is quite high for BL Lac (3.8σ), while it is only marginal for OJ 287 (2.3σ). The relatively low flux for the latter source is at the level expected from background fluctuations, and therefore we do not regard this detection as real.

Table 3 reports the results of a single power-law fits including the data from all the three Narrow Field Instruments for BL Lac. The normalization factor between PDS and MECS was fixed at 0.86, as derived from intercalibration tests performed on known sources (see the SDC Handbook). The PDS points are compatible with the best fit of the LECS and MECS data, even if slightly above the model.

Because of the absence of imaging capabilities, the PDS spectra can be contaminated by serendipitous sources in its field of view. We therefore first checked the MECS image of BL Lac for the presence of other sources, founding two in the field but with count rates a factor of 10 and 40 fainter than the target. However, given its wide field of view ($\sim 1.4^\circ$ FWHM), larger than the LECS and MECS ones ($\sim 28'$ for the MECS), there is also the possibility of a contamination by hard serendipitous sources not visible in the MECS images. We therefore checked WGACAT, the publicly available database of ROSAT sources (White, Giommi, & Angelini 1995), for serendipitous X-ray sources within $\sim 90'$ from BL

Lac. We found five, but all of them were at least an order of magnitude fainter than our target, and with relatively steep spectral indices (derived from the hardness ratios). It then follows that it is very unlikely that any of these sources can contribute significantly to the PDS flux of BL Lac, although the possibility remains that some hard X-ray sources might not have been detected by ROSAT.

4.3 Notes on individual sources

PKS 1144–379. LECS data below 1 keV present a clear trend, suggesting a steep spectral index with stronger evidence than that provided by the F-test, given the few points involved. MECS data present a feature around 4 keV but given the available S/N and resolution it is hard to assess the reality of this feature.

OJ 287. MECS data seem to show an emission feature around 2.3 keV but, again, the low S/N does not allow reliable conclusions to be drawn.

The X-ray spectral index we obtain ($\alpha_x = 0.6 \pm 0.2$) agrees with the value derived by Kubo et al. (1998) of 0.62 ± 0.01 , based on ASCA observations made in November 1994. Our flux, however, is $\sim 50\%$ smaller.

PKS 2005–489. This source experienced a pronounced flare in November 1998, about two years after our *Bep-*

poSAX observations. Tagliaferri et al. (2001) observed it with *BeppoSAX* on November 1–2 and fitted a single power-law to the data over the 0.1 – 200 keV range with $\alpha_x = 1.18 \pm 0.02$ and free N_H . This is slightly flatter than our value of 1.33 ± 0.04 , derived between 1 and 10 keV (as we do not have LECS data) and assuming a Galactic N_H close to their best-fit free N_H (see also Fig. 6). Their data actually require a broken power-law with a break around 2 keV and a steepening $\Delta\alpha_x \sim 0.2$ at higher energies. Their X-ray flux was ~ 3 times higher than our value. Perlman et al. (1999) followed the evolution of the flare between October 14 and December 31 when the X-ray flux changed by a factor of four. The X-ray spectral index in the 2 – 10 keV band also varied between 1.3 and 1.8.

BL Lac. Our results are consistent with those of Sambruna et al. (1999), based on ASCA observations obtained in November 1995. Their single power-law fit, assuming the same (fixed) N_H value, has an energy index $\alpha_x = 1.08 \pm 0.03$, to be compared with our value of 0.96 ± 0.08 . Their 1 keV flux, derived for their fit with free N_H , and their broken power-law fit are also consistent with ours. This shows that by the time of our *BeppoSAX* observations (Nov. 1997) the source had returned to its pre-flare status. In July 1997, in fact, during its optical/X-ray/ γ -ray flare, the X-ray flux of BL Lac was ~ 3 times higher, with a much flatter X-ray spectrum ($\alpha_x \sim 0.4 - 0.7$; Tanihata et al. 2000; see also Fig. 6).

5 ROSAT PSPC DATA

In order to compare our results with previous (soft) X-ray observations and especially to take advantage of the higher resolution and collecting area at low energies, we used data from the ROSAT Position Sensitive Proportional Counter (PSPC) public archive. The 1 Jy BL Lac ROSAT data had been originally published by Urry et al. (1996), while those for B2 0912+29 were published by Lamer et al. (1996). In order to ensure a uniform procedure for the whole sample, we have re-analyzed all ROSAT data, obtaining results consistent within the errors with those already published.

The journal of the ROSAT observations is given in Table 4. The basic event files from the archive have been corrected for gain variations on the detector surface with the program PCSASSCORR in FTOOLS, when not already done by the Standard Reduction process (SASS version 7.8 and later, M. Corcoran, private communication). Since all the sources were ROSAT targets a standard extraction radius of $3'$ ($2.5'$ when serendipitous sources were present in the field or when the source was particularly weak) was used, to avoid the possible loss of soft photons due to the ghost imaging effect. We have used the appropriate response matrices for the different gain levels of the PSPC B detector before and after 14 Oct. 1991 (gain1 and gain 2, respectively). The background has been evaluated in two circular regions (of radius $\sim 20 - 30$ pixels) away from the central region and from other serendipitous sources, but inside the central rib ring of the detector. The spectra have been rebinned (using GRPPHA) to have at least 20 net counts in every new bin, to justify the use of χ^2 statistics. Channel 1-11 and 212-256 have been excluded from the analysis, due to calibration uncertainties.

As for the *BeppoSAX* data, we fitted the ROSAT PSPC data with a single power-law model with Galactic and free absorption. Our results are presented in Table 5, which gives the name of the source in column (1), N_H in column (2), the energy index α_x in column (3), the 1 keV flux in μJy in column (4), the unabsorbed 0.1 – 2.4 keV flux in column (5), the reduced chi-squared and number of degrees of freedom, $\chi^2/(\text{dof})$ in column (6), and the observing date in column (7). The errors quoted on the fit parameters are the 90% uncertainties for one and two interesting parameters, for Galactic and free N_H respectively. The errors on the 1 keV flux reflect the statistical errors only and not the model uncertainties.

Table 5 shows that the fitted N_H values are consistent with the Galactic ones for most sources; this is confirmed by an *F*-test which shows that the addition of N_H as a free parameter does not result in a significant improvement in the χ^2 values. The fit for PKS 2005–489 is not particularly good, especially for Galactic N_H . The fact that the free N_H value is lower than the Galactic one suggests the presence of a “soft excess”. Indeed, Comastri et al. (1997) fitted a broken-power law model to these data, with a steep soft index $\sim 4.7 - 4.8$. The fitted energy indices are relatively steep (apart from 4C 56.27). The mean value is $\langle\alpha_x\rangle = 1.44 \pm 0.22$, the weighted mean is $\langle\alpha_x\rangle = 2.01 \pm 0.02$. This latter value is clearly dominated by PKS 2005–489, an HBL with a very well determined slope. Excluding this source and 4C 56.27 we derive a mean value $\langle\alpha_x\rangle = 1.51 \pm 0.14$, with a weighted mean $\langle\alpha_x\rangle = 1.53 \pm 0.03$.

5.1 Comparison between *BeppoSAX* and ROSAT results

Figure 3 shows the *BeppoSAX* 1 keV flux versus the corresponding ROSAT flux. The errors reflect statistical uncertainties only and do not include model uncertainties. Our sources display mild X-ray variability: the median value of $f_{\text{BeppoSAX}}/f_{\text{ROSAT}}$ is 0.6 (0.5 excluding PKS 2005–489 which has the largest value of this ratio, ~ 5). Fig. 3 should be compared with Fig. 2 in Wolter et al. (1998), which shows the same plot for a sample of eight HBL. There the two fluxes are within 30% for most sources and the points follow more closely the line of equal fluxes. We note that the 1 keV flux has a very strong model dependence. We therefore evaluated the X-ray flux ratio also in the 0.1 – 2.4 keV range, a band common to both instruments and less model dependent. The median value in this case is not very different, $f_{\text{BeppoSAX}}/f_{\text{ROSAT}} = 0.4$.

Figure 4 shows the *BeppoSAX* spectral index (0.1 – 10 keV) vs. the ROSAT spectral index (0.1 – 2.4 keV). The larger *BeppoSAX* error bars for most of our sources, as compared to ROSAT, are due to the worse photon statistics. (The PSPC count rates, in fact, are typically a factor of 10 larger than the LECS ones.) All but one source occupy the region of the plot where $\alpha_x(\text{BeppoSAX}) \leq \alpha_x(\text{ROSAT})$. The interpretation of this plot is complicated by variability effects, which affect the shape of the X-ray spectrum, and possibly by ROSAT miscalibrations (e.g., Iwasawa, Fabian & Nandra 1999; Mineo et al. 2000). However, a few points can be made. Again, as before, the figure suggests a concave overall X-ray spectrum for our sources, with a flatter component emerging at higher energies. We find

Table 4. ROSAT journal of observations

Name	exposure sec.	full band net count rate (cts/s)	Observing Date
PKS 0048–097	8359	0.408 ± 0.007	1993 Jul 4-15
OJ 287	3566	0.285 ± 0.010	1991 Apr 16
	6702	0.602 ± 0.010	1991 Nov 10-11
	3277	0.621 ± 0.014	1993 Oct 19
B2 0912+29	2809	0.428 ± 0.013	1991 Apr 24 - May 6
PKS 1144–379	7745	0.115 ± 0.004	1993 Jul 7-8
PKS 1519–273	2548	0.106 ± 0.008	1993 Aug 17-18
4C 56.27	5896	0.138 ± 0.005	1992 Jun 19-20
PKS 2005–489	11320	2.760 ± 0.016	1992 Apr 27-29
	11457	1.667 ± 0.012	1992 Oct 28 - Nov 1
BL Lac	2167	0.176 ± 0.010	1992 Dec 22-23

Table 5. ROSAT PSPC, single power-law fits

Name	N_{H} 10^{20} cm^{-2}	α_{x}	$F_{1\text{keV}}$ μJy	$F_{[0.1-2.4]}$ $\text{erg cm}^{-2} \text{ s}^{-1}$	χ^2/dof	Observing Date
PKS 0048–097	3.85 fixed	1.63 ± 0.04	0.86 ± 0.03	$1.22\text{e-}11$	0.76/55	1993 Jul 4-15
	$4.39^{+0.60}_{-0.58}$	1.79 ± 0.19	0.87 ± 0.04	$1.52\text{e-}11$	0.70/54	
OJ 287	2.75 fixed	$1.17^{+0.08}_{-0.08}$	$0.61^{+0.04}_{-0.04}$	$5.34\text{e-}12$	0.79/31	1991 Apr 16
	$2.71^{+1.06}_{-0.92}$	$1.15^{+0.36}_{-0.33}$	$0.61^{+0.05}_{-0.05}$	$5.27\text{e-}12$	0.82/30	
	2.75 fixed	$1.62^{+0.04}_{-0.04}$	$0.97^{+0.04}_{-0.04}$	$1.34\text{e-}11$	0.89/80	1991 Nov 10-11
	$2.37^{+0.44}_{-0.41}$	$1.47^{+0.17}_{-0.17}$	$0.96^{+0.04}_{-0.04}$	$1.14\text{e-}11$	0.86/79	
B2 0912+29	2.11 fixed	$1.53^{+0.08}_{-0.08}$	$0.60^{+0.05}_{-0.05}$	$7.46\text{e-}12$	0.75/31	1991 Apr 24 - May 6
	$1.64^{+0.78}_{-0.64}$	$1.34^{+0.33}_{-0.29}$	$0.59^{+0.05}_{-0.05}$	$6.05\text{e-}12$	0.72/30	
PKS 1144–379	7.64 fixed	$1.37^{+0.14}_{-0.14}$	$0.41^{+0.03}_{-0.03}$	$4.41\text{e-}12$	1.04/16	1993 Jul 7-8
	$10.0^{+3.9}_{-2.3}$	$1.71^{+0.41}_{-0.23}$	$0.45^{+0.05}_{-0.04}$	$7.08\text{e-}12$	0.78/15	
PKS 1519–273	8.66 fixed	$1.12^{+0.26}_{-0.29}$	$0.40^{+0.05}_{-0.05}$	$3.35\text{e-}12$	1.56/10	1993 Aug 17-18
	$32.7^{+55.5}_{-22.3}$	$2.86^{+3.37}_{-1.63}$	$0.84^{+1.71}_{-0.80}$	$7.91\text{e-}11$	0.95/9	
4C 56.27	4.16 fixed	$0.23^{+0.15}_{-0.15}$	$0.45^{+0.03}_{-0.03}$	$2.51\text{e-}12$	0.79/23	1992 Jun 19-20
	$5.63^{+3.41}_{-1.99}$	$0.46^{+0.40}_{-0.40}$	$0.47^{+0.03}_{-0.05}$	$2.79\text{e-}12$	0.52/22	
PKS 2005–489	5.08 fixed	$2.25^{+0.02}_{-0.02}$	$5.15^{+0.07}_{-0.07}$	$1.74\text{e-}10$	2.15/89	1992 Apr 27-29
	$4.28^{+0.19}_{-0.19}$	$1.99^{+0.06}_{-0.06}$	$5.12^{+0.07}_{-0.07}$	$1.18\text{e-}10$	1.25/88	
	5.08 fixed	$2.43^{+0.02}_{-0.02}$	$2.70^{+0.05}_{-0.05}$	$1.22\text{e-}10$	3.48/65	1992 Oct 28 - Nov 1
	$3.54^{+0.23}_{-0.23}$	$1.91^{+0.08}_{-0.08}$	$2.71^{+0.03}_{-0.05}$	$5.54\text{e-}11$	0.79/64	
BL Lac	36.0 fixed	$2.13^{+0.36}_{-0.36}$	$1.55^{+0.14}_{-0.14}$	$4.38\text{e-}11$	0.56/11	1992 Dec 22-23
	$33.7^{+4.58}_{-2.44}$	$2.01^{+2.35}_{-1.49}$	$1.45^{+1.50}_{-0.62}$	$3.43\text{e-}11$	0.62/10	

Note: the errors are at 90% confidence level for one (with fixed N_{H}) and two parameters of interest.

$\alpha_{\text{x}}(\text{ROSAT}) - \alpha_{\text{x}}(\text{BeppoSAX}) = 0.47 \pm 0.23$ (excluding the two HBL this becomes $\alpha_{\text{x}}(\text{ROSAT}) - \alpha_{\text{x}}(\text{BeppoSAX}) = 0.43 \pm 0.30$). This difference cannot be attributed to miscalibration effects alone which, if present, should steepen the ROSAT slopes by $\sim 0.2 - 0.3$ (Mineo et al. 2000).

Again, this figure should be compared with Fig. 3 of

Wolter et al. (1998), which shows the same plot for a sample of 8 HBL. In that case the *BeppoSAX* and ROSAT spectral indices agree within the errors for all but one source.

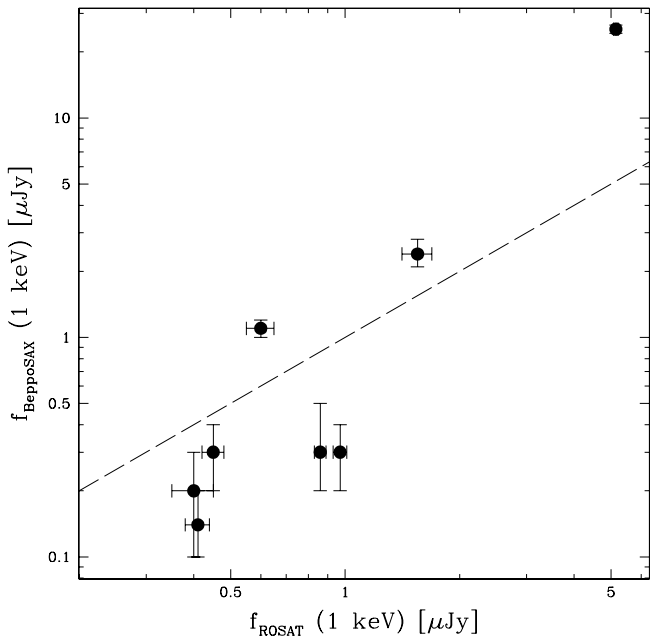


Figure 3. The 1 keV X-ray flux from our *BeppoSAX* data vs. the 1 keV X-ray flux from ROSAT data. The dashed line represents the locus of $f_{BeppoSAX} = f_{ROSAT}$. The errors reflect the statistical errors only and not the model uncertainties. For OJ 287 and PKS 2005–489, which have multiple ROSAT observations, we took the observation with the largest X-ray flux (Oct. 1993 and Apr. 1992 respectively).

6 SPECTRAL ENERGY DISTRIBUTIONS

To address the relevance of our *BeppoSAX* data in terms of emission processes in BL Lacs, we have assembled multifrequency data for all our sources. The main source of information was NED, and so most data are not simultaneous with our *BeppoSAX* observations. For five of our sources, however, we were able to find nearly-simultaneous (within a month) radio observations in the University of Michigan Radio Astronomy Observatory (UMRAO) database. These are reported in Table 6, which also gives the nearly-simultaneous radio-X-ray spectral index, α_{rx} with its error. This is defined between the rest-frame frequencies of 4.8 GHz and 1 keV, and has been K-corrected using the X-ray spectral indices given in Table 3 and radio spectral indices between 4.8 and 8.0 GHz derived from the UMRAO data ($z = 0.3$ was assumed for the two sources in the table without redshift information). Three of our sources were also detected by EGRET so their energy distributions reach $\sim 5 \times 10^{24}$ Hz. The EGRET data come from the compilation of Lin et al. (1999), which include the first entries in the Third EGRET Catalog.

The spectral energy distributions (SEDs) for our sources are shown in Figures 5 and 6, where filled circles indicate *BeppoSAX* data and the nearly-simultaneous radio data and open symbols typically represent non-simultaneous literature (NED) data. The *BeppoSAX* data have been converted to νf_ν units using the XSPEC unfolded spectra after correcting for absorption. ROSAT (from Tab. 5) and

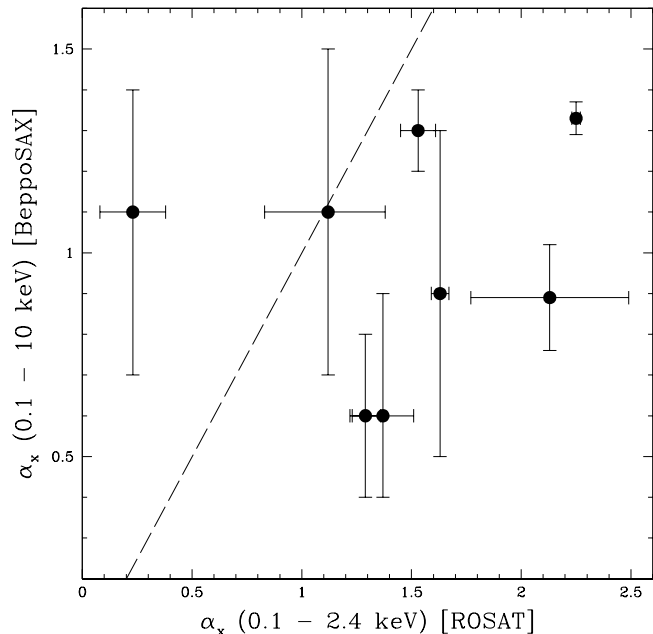


Figure 4. The *BeppoSAX* spectral index (0.1 – 10 keV) vs. the ROSAT spectral index (0.1 – 2.4 keV). The dashed line represents the locus of $\alpha_x(BeppoSAX) = \alpha_x(ROSAT)$. For OJ 287 and PKS 2005–489, which have multiple ROSAT observations, we took the observation with the largest X-ray flux (Oct. 1993 and Apr. 1992 respectively).

EGRET data are shown by a bow-tie that represent the spectral index range.

We have fitted a homogeneous, one-zone synchrotron inverse Compton model to the SED of our sources. The model is very similar to the one described in detail in Spada et al. (2001; it is the “one-zone” version of it). It assumes that the source is cylindrical, of size R and width $\Delta R' = R/\Gamma$ (in the comoving frame, where Γ is the bulk Lorentz factor). The particle distribution $N(\gamma)$ is assumed to have the slope n [$N(\gamma) \propto \gamma^{-n}$] above the random Lorentz factor γ_c , where radiative losses dominate over adiabatic losses. The electron distribution is assumed to cut-off abruptly at $\gamma_{max} > \gamma_c$. Below γ_c there can be two cases, depending on the values of γ_c and γ_{min} . If $\gamma_c > \gamma_{min}$, we have $N(\gamma) \propto \gamma^{-n+1}$ between γ_{min} and γ_c and $N(\gamma) \propto \gamma^{-1}$ below γ_{min} . Alternatively, if $\gamma_c < \gamma_{min}$, then $N(\gamma) \propto \gamma^{-2}$ between γ_c and γ_{min} and γ^{-1} below γ_c . According to these assumptions, the random Lorentz factor of the electrons emitting most of the radiation (i.e., emitting at the peaks of the SEDs), γ_{peak} , is determined by the relative importance of the adiabatic versus radiative losses and can assume values in the range $\gamma_{min} - \gamma_{max}$.

Photons produced externally to the jet (e.g., by the broad line region; BLR) are considered only if they improve the fit. We account for them assuming that a fraction 0.1 of the disk luminosity L_{disk} is reprocessed into line emission by the BLR assumed to be located at R_{BLR} . The source is assumed to emit an intrinsic luminosity L' and to be observed with the viewing angle θ . The input parameters are listed in Table 7, which gives the name of the source in column (1), L' in column (2), L_{disk} in column (3), R_{BLR} in column (4),

the magnetic field B in column (5), the size of the region R in column (6), the Lorentz factor Γ in column (7), the angle θ in column (8), the slope of the particle distribution n in column (9), and finally γ_{\min} and γ_{peak} in columns (10) and (11) respectively. Note that γ_{peak} is a derived quantity and not an input parameter.

In the case of a pure synchrotron self-Compton model, all the above parameters are constrained in sources for which: 1) we have an estimate of the minimum timescale of variability; 2) both the synchrotron and the self-Compton peak are well defined; 3) the spectral slopes before and above the peaks are known; 4) the redshift is known. As discussed in Tavecchio, Maraschi & Ghisellini (1998), this suffices to fix the values of the magnetic field, the intrinsic power of the source, the slopes of the emitting electron distribution, the relativistic Doppler factor, and the dimension of the source. When the radiation produced externally to the jet is important there is one unconstrained unknown, but the superluminal motion of the radio knots observed for many of these sources indicates values of the bulk Lorentz factor in the range 10–15 on average, and we therefore use these values for our fits (see, e.g., Ghisellini et al. 1998).

For the sources in our sample, we rarely have complete information about the high-energy peak (we often have only an upper limit), so we lack the direct determination of γ_{peak} and have only a limit on the determination of the magnetic field.

But in the model we use here the adiabatic losses play a crucial role, and (within this model) we have an additional constrain with respect to the simplest synchrotron inverse Compton model. Namely, the peak of the synchrotron emission is either due to the electrons injected with γ_{\min} , or it is due to the electrons for which adiabatic and radiative losses balance. This second condition (coupled with the value of the synchrotron peak frequency) allows to estimate the value of the magnetic field, since for our sources the synchrotron energy losses are important (as shown by the upper limits in the EGRET energy range indicating an inverse Compton emission not widely dominant).

A further constraint applies to sources in which external radiation could be important. In our model these external seed photons are thought to be produced by the broad line region, reprocessing a fixed amount of the ionizing flux produced by the accretion disk. Therefore the accretion disk luminosity has not to exceed the observed optical–UV continuum (for our sources we do not have any evidence for the presence of a blue bump), nor the emission line luminosities have to exceed the observed values.

The model fits are shown in Fig. 5 and 6 as solid (and dashed) lines. The applied model is aimed at reproducing the spectrum originating in a limited part of the jet, thought to be responsible for most of the emission. This region is necessarily compact, since it must account for the fast variability shown by all blazars, especially at high frequencies. The radio emission from this compact regions is strongly self-absorbed, and the model cannot account for the observed radio flux. This explains why the radio data are systematically above the model fits in the figures.

For some sources the model fits present a complex behavior at γ -ray energies (i.e., two peaks at high energies besides the synchrotron peak at lower frequencies). In all such cases the first high energy peak is due to synchrotron

self-Compton emission, while the peak at the highest energies is due to inverse Compton off external photons.

As shown in Table 7, the intrinsic luminosities, the source dimensions, the bulk Lorentz factors and the viewing angles are quite similar for all sources, while the magnetic field varies from 0.8 to 6 Gauss (with the smallest values corresponding to the least powerful sources). The need for external seed photons for some sources, while indicative of a broad line region, is not extremely compelling, since the required disk luminosities are much smaller than those required in radio-loud quasars (see, e.g., Ghisellini et al. 1998). The main difference between sources are in the derived value of γ_{peak} with HBL having, not surprisingly, the larger values. Moreover, γ_{peak} strongly (anti-)correlates with L' , that is powerful sources have the smallest values of γ_{peak} , in agreement with what previously found by Ghisellini et al. (1998).

7 X-RAY SPECTRAL INDEX AND THE SYNCHROTRON PEAK FREQUENCY

One of the aims of this project was to study the dependence of the X-ray spectral index on the synchrotron peak frequency ν_{peak} found by Padovani & Giommi (1996) and Lamer et al. (1996) from ROSAT data by using the broader *BeppoSAX* energy band. Padovani & Giommi (1996) found a strong anti-correlation between α_x and ν_{peak} for HBL (i.e., the higher the peak frequency, the flatter the spectrum), while basically no correlation was found for LBL. This was interpreted as due to the tail of the synchrotron component becoming increasingly dominant in the ROSAT band as ν_{peak} moves closer to the X-ray band (see Fig. 7 of Padovani & Giommi 1996).

The *BeppoSAX* version of this dependence is shown in Figure 7, which plots the X-ray spectral index (0.1 – 10 keV) vs. the logarithm of the peak frequency for our sources (filled circles), the HBL studied by Wolter et al. (1998; open squares), and other BL Lacs studied by *BeppoSAX*. These include, in order of increasing peak frequency: ON 231 (star; α_x in the 0.1 – 3.8 keV range; Tagliaferri et al. 2000), S5 0716+714 (open circle; Giommi et al. 1999), PKS 2155–304 (filled triangle; Giommi et al. 1998), MKN 421 (cross; α_x in the 0.1 – 1.6 keV range; Fossati et al. 2000), 1ES 2344+514 (open triangle; Giommi, Padovani & Perlman 2000), and MKN 501 (filled square; Pian et al. 1998). When more than a value of α_x was available for these BL Lacs we picked the one corresponding to the largest ν_{peak} . The ν_{peak} values for the sources studied in this paper have been taken from Sambruna, Maraschi & Urry (1996), who fitted a parabola to the νf_ν broad-band spectra, except for B2 0912+29 and PKS 2005–489. For these two sources we derived ν_{peak} as described in Padovani & Giommi (1996). The former source, in fact, was not included in the sample studied by Sambruna et al. (1996), while for the latter the derived value was clearly too high (see, e.g., Comastri, Molendi & Ghisellini 1995). The ν_{peak} values for the HBL studied by Wolter et al. (1998) are taken from that paper and similarly the values for the additional sources are normally taken from the referenced papers.

Fig. 7, although with less statistics, basically confirms the ROSAT findings, namely a strong anti-correlation between α_x and ν_{peak} for HBL and no correlation for LBL,

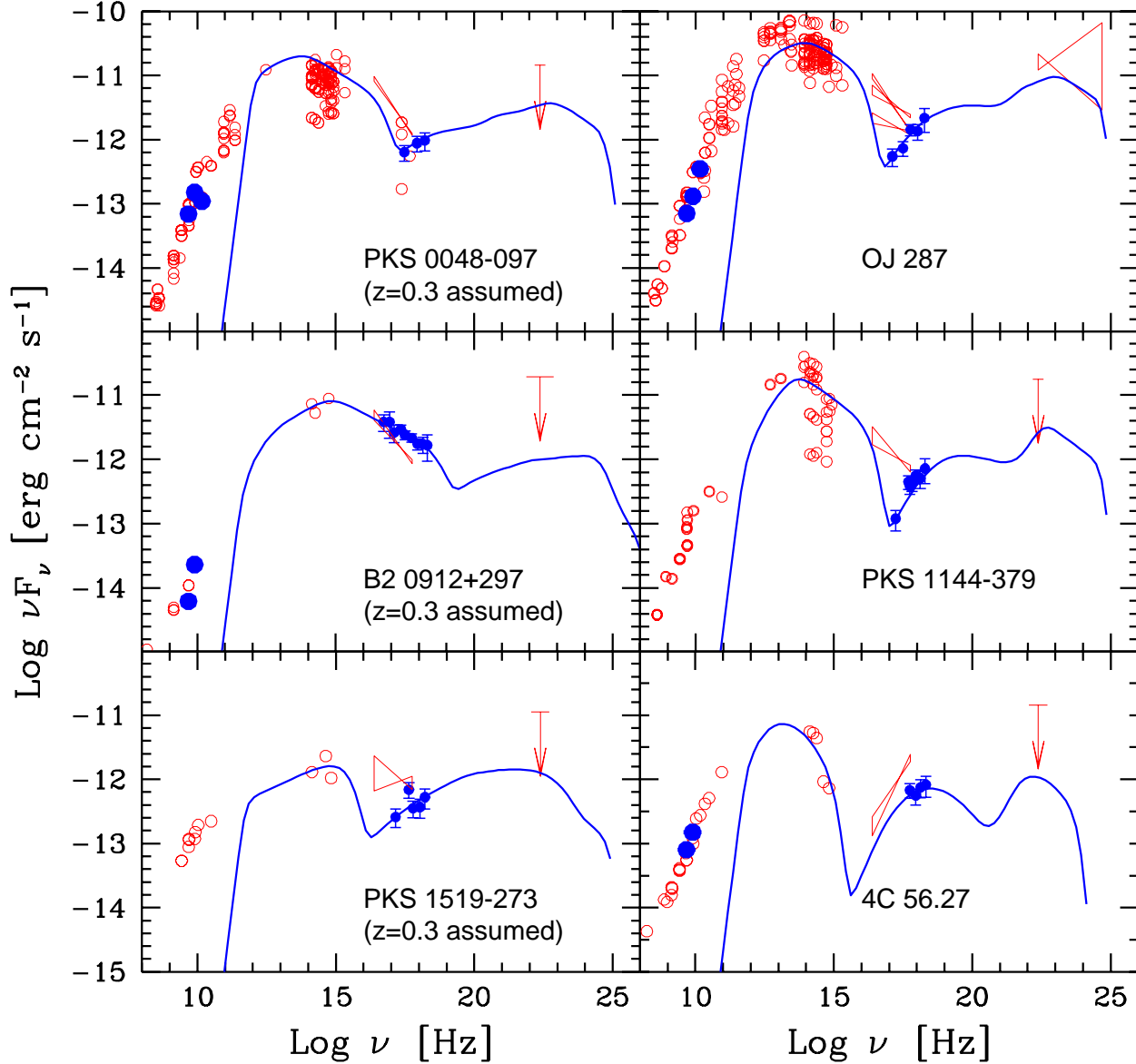


Figure 5. Spectral energy distributions of six of our sources. Filled symbols indicate *BeppoSAX* data and nearly-simultaneous radio data from UMRAO, while open symbols indicate data from the literature (NED). The solid lines correspond to the one-zone homogeneous synchrotron and inverse Compton model calculated as explained in the text, with the parameters listed in Table 7.

Table 6. Nearly-simultaneous Radio Observations

Name	$F_{4.8\text{GHz}}$ Jy	Observing date	$F_{8.0\text{GHz}}$ Jy	Observing date	$F_{14.5\text{GHz}}$ Jy	Observing date	α_{rx}
PKS 0048–097	1.43 ± 0.04	1997 Dec 3	1.83 ± 0.19	1997 Dec 6	0.79 ± 0.06	1997 Dec 16	0.85 ± 0.03
OJ 287	1.47 ± 0.05	1997 Nov 15	1.63 ± 0.08	1997 Nov 25	2.44 ± 0.05	1997 Dec 17	0.86 ± 0.02
B2 0912+29	0.13 ± 0.03	1997 Dec 2	0.29 ± 0.04	1997 Dec 8	0.62 ± 0.01
4C 56.27	1.66 ± 0.07	1997 Oct 18	1.87 ± 0.09	1997 Oct 7	0.84 ± 0.02
BL Lac	3.73 ± 0.13	1997 Nov 9	4.53 ± 0.12	1997 Nov 21	4.47 ± 0.12	1997 Nov 13	0.80 ± 0.01

with an initial increase in α_x going from LBL to HBL. A few differences, however, are worth mentioning. First, the range in α_x is somewhat smaller (~ 1 vs. ~ 3). This is likely due to the larger energy range over which α_x is measured (0.1 – 10 keV for *BeppoSAX* vs. 0.1 – 2.4 keV for

ROSAT). Objects with very steep ROSAT α_x , in fact, are those in which synchrotron emission is nearing the exponential cut-off; by having a larger band *BeppoSAX* includes flatter, higher energy emission due to inverse Compton. Second, the wide 0.1 – 100 keV coverage of *BeppoSAX* has allowed

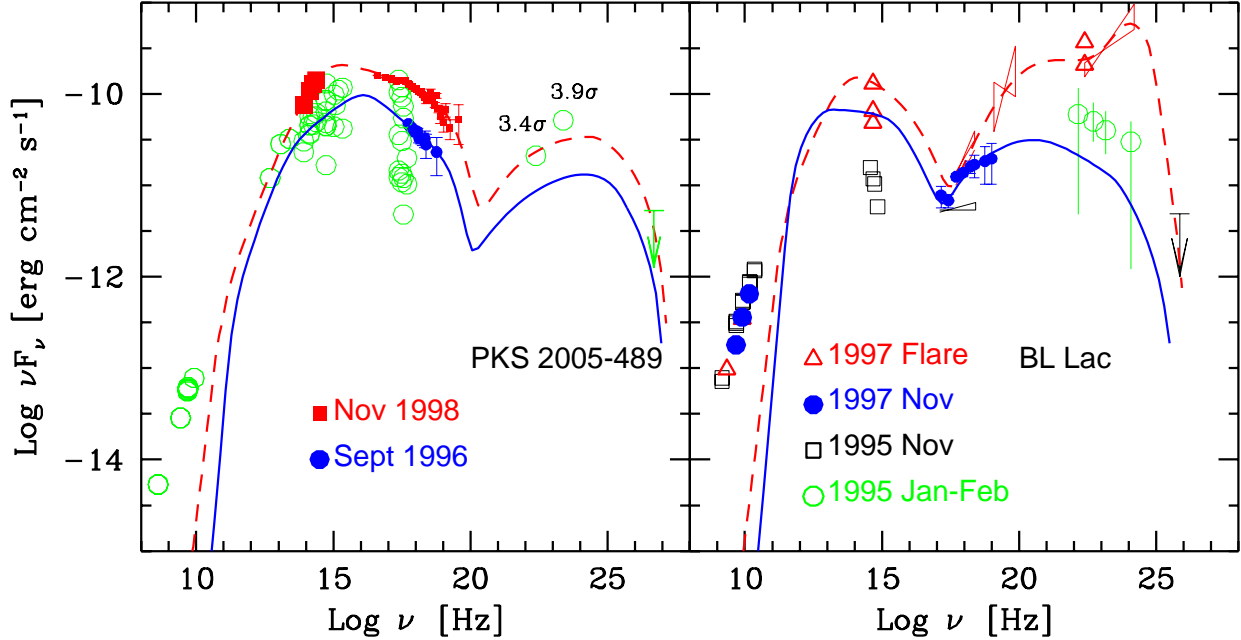


Figure 6. Spectral energy distributions of PKS 2005–489 and BL Lac. PKS 2005–489: filled circles indicate our *BeppoSAX* data (Sept. 1996), while filled squares represent the *BeppoSAX* observations of November 1998, with simultaneous infrared data (Tagliaferri et al. 2001); open symbols indicate data from the literature (NED). BL Lac: filled circles indicate our *BeppoSAX* data (Nov. 1997) and nearly-simultaneous radio data from UMRAO, other points correspond to different observing dates, with triangles indicating the summer 1997 flare (see Sambruna et al. 1999 for details on the various data). The lines (solid: our data; dashed: other campaigns) correspond to the one-zone homogeneous synchrotron and inverse Compton model calculated as explained in the text, with the parameters listed in Table 7.

Table 7. Model Input Parameters

Name	L' erg s $^{-1}$	L_{disk} erg s $^{-1}$	R_{BLR} cm	B G	R cm	Γ	θ	n	γ_{min}	γ_{peak}
PKS 0048–097	3.0e42	1e45	6e17	5	1.6e16	12	4.5	3.5	50	560
OJ 287	3.0e42	1e45	5e17	5	1.3e16	13	4	3.5	150	660
B2 0912+29	8.0e41	1e44	5e17	3	1.2e16	13	4	3.45	200	2300
PKS 1144–379	6.0e42	6e44	5e17	6	2.0e16	15	3	3.6	400	400
PKS 1519–273	5.0e41	0.8	1.0e16	13	4.7	3.6	40	10,000
4C 56.27	6.0e42	5e44	5e17	5	2.0e16	13	5	3.95	200	500
PKS 2005–489	2.0e41	1.5	1.0e16	13	3	3.5	600	12,000
BL Lac	1.1e42	1.2	1.5e16	10	5.	4.05	300	300

the detection of spectacular spectral variability with ν_{peak} reaching $\gtrsim 10$ keV. As predicted by Padovani & Giommi (1996), these sources display very flat α_x ($\sim 0.5 - 0.8$), since *BeppoSAX* is sampling the peak of the synchrotron emission. Note that in this case the flat X-ray spectrum is *not* associated with inverse Compton emission, although extreme HBL (objects to the far right in Fig. 7) have synchrotron X-ray spectra as flat as extreme LBL (objects to the far left of the figure). In other words, there are two very different mechanisms which can produce a flat X-ray spectrum in BL Lacs: inverse Compton emission or synchrotron emission with peak frequency in the hard X-ray band.

8 RESULTS AND CONCLUSIONS

We have presented new *BeppoSAX* observations of eight BL Lacertae objects, all but one selected from the 1 Jy sample. Six of our sources are LBL, i.e., they are characterized by a peak in their multifrequency spectra at infrared/optical energies. A relatively simple picture comes out from this paper: a dominance of inverse Compton emission in the X-ray band of LBL, with $\sim 2/3$ of the sources showing also a likely synchrotron component. This result rests on various pieces of evidence:

- the relatively flat ($\alpha_x \sim 0.9$) *BeppoSAX* spectra of our LBL sources (Tab. 3). Moreover, single power-law fits to the *BeppoSAX* data show a best fit N_{H} below the Galactic value for four out of six of our LBL, while residuals to the single power-law fits with Galactic N_{H} also show evidence for

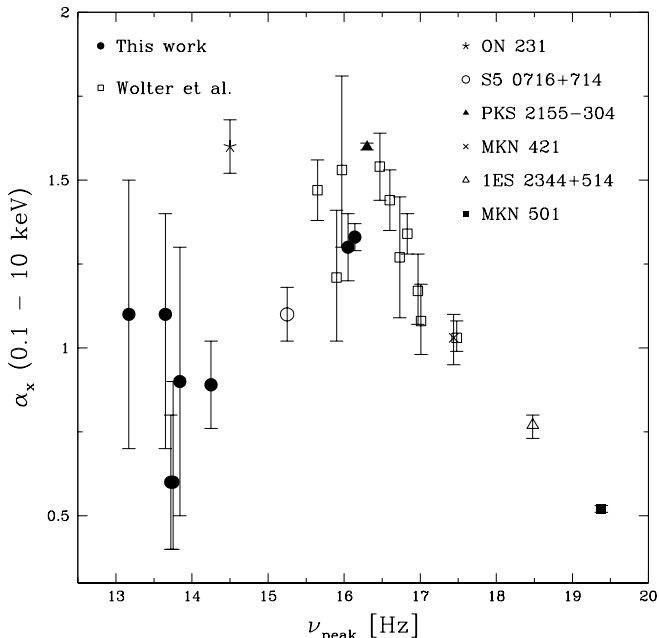


Figure 7. The *BeppoSAX* spectral index (0.1 – 10 keV) vs. the logarithm of the peak frequency for our sources (filled circles), the HBL studied by Wolter et al. (1998; open squares), ON 231 (star), S5 0716+714 (open circle), PKS 2155–304 (filled triangle), MKN 421 (cross), 1ES 2344+514 (open triangle), and MKN 501 (filled square). See text for details and references.

concave spectra (Fig. 2). Broken power-law models improve the fits but with border-line significance. The resulting best-fits, however, all concur in indicating a flatter component emerging at higher energies, with spectral changes $\Delta\alpha_x \sim 0.8$ around 1 – 3 keV.

- the comparison between *BeppoSAX* and ROSAT spectra (Fig. 4). Excluding 4C 56.27, which appears to have an extremely flat ROSAT spectrum, all our LBL have $\alpha_x(\text{ROSAT}) > \alpha_x(\text{BeppoSAX})$, with a typical difference ~ 0.7 . Although the interpretation of this difference is complicated by possible spectral variability effects, it is unlikely that these can explain the fact that five out of six of our LBL have a ROSAT spectrum which is steeper than the *BeppoSAX* one. Similarly, possible ROSAT miscalibrations, if at all present, could only explain a difference $\sim 0.2 - 0.3$.

- the spectral energy distributions (Fig. 5 and 6). Despite the non-simultaneity of the multifrequency data (UMRAO radio data excluded) it is apparent that the *BeppoSAX* spectra indicate a different emission component in the SEDs of our LBL sources, separate from that responsible for the low energy emission. In fact, the extrapolation of the relatively flat *BeppoSAX* slopes cannot be extended to much lower frequencies since the predicted optical flux would be orders of magnitude below the observed value. A sharp steepening towards lower frequencies is then necessary to meet the much higher optical (synchrotron) flux, as also required by the comparison with ROSAT data. Detailed synchrotron inverse Compton model fits to the SEDs fully confirm this picture and constrain the physical parameters in these sources (Tab. 7).

- the $\alpha_x - \nu_{\text{peak}}$ diagram (Fig. 7). Our interpretation

of this plot is the one originally proposed by Padovani & Giommi (1996) for the ROSAT data. Namely, α_x is flat for LBL due to the dominance of the inverse Compton emission, and steepens moving from LBL to HBL as synchrotron replaces inverse Compton as the main emission mechanism in the X-ray band. The spectral index then flattens again as the synchrotron peak moves to higher energies in the X-ray band, eventually converging to the relatively flat value characteristic of synchrotron emission before the peak. Again, this fits perfectly with a dominance of inverse Compton emission in our LBL.

Note that strong, direct evidence for the presence of both synchrotron and inverse Compton emission in the *BeppoSAX* spectra of LBL has been presented by Giommi et al. (1999) and Tagliaferri et al. (2000) for S5 0716+714 and ON 231, respectively. All data for the two HBL included in this study are consistent with synchrotron emission extending into the *BeppoSAX* band for these sources, in agreement with the results of Wolter et al. (1998).

BeppoSAX data for four more 1 Jy BL Lacs have been obtained and data reduction is in progress. Those results will be presented in a forthcoming paper, where we will address the properties of the full 1Jy *BeppoSAX* sample and their physical parameters in more details.

ACKNOWLEDGEMENTS

We thank F. Fiore for providing the code to de-redden the XSPEC unfolded spectra used to construct the spectral energy distribution plots and Tommaso Maccacaro, Franco Mantovani, and Carlo Stanghellini for their contribution at an early stage of this project. AC acknowledges financial support from ASI-ARS-99-75 while LC acknowledges the STScI Visitor Program. This research has made use of data from the University of Michigan Radio Astronomy Observatory which is supported by funds from the University of Michigan and of the NASA/IPAC Extragalactic Database (NED), which is operated by the Jet Propulsion Laboratory, California Institute of Technology, under contract with the National Aeronautics and Space Administration.

REFERENCES

- Boella G. et al. , 1997a, A&AS, 122, 299
 Boella G. et al. , 1997b, A&AS, 122, 327
 Comastri A., Molendi S., Ghisellini G., 1995, MNRAS, 277, 297
 Comastri A., Fossati G., Ghisellini G., Molendi S., 1997, ApJ, 480, 534
 Dickey J. M., Lockman F. J., 1990, ARAA, 28, 215
 Elvis M., Lockman F. J., Wilkes, B. J., 1989, AJ, 97, 777
 Fossati G., Maraschi L., Celotti A., Comastri A., Ghisellini G., 1998, MNRAS, 299, 433
 Fossati G. et al., 2000, ApJ, 541, 166
 Frontera F. et al., 1997, A&AS, 122, 357
 Gehrels N., 1986, ApJ, 303, 336
 Ghisellini G., Celotti A., Fossati G., Maraschi L., Comastri A., 1998, MNRAS, 301, 451
 Giommi P., Fiore, F., 1997, in 5th International Workshop on Data Analysis in Astronomy, Erice, in press
 Giommi P. et al., 1998, A&A, 333, L5
 Giommi P. et al., 1999, A&A, 351, 59

- Giommi P., Padovani P., 1994, MNRAS, 268, L51
 Giommi P., Padovani P., Perlman E., 2000, MNRAS, 317, 743
 Heidt J., Wagner S. J., 1996, A&A, 305, 42
 Iwasawa K., Fabian A. C., Nandra K., 1999, MNRAS, 307, 611
 Kollgaard R. I., 1994, Vistas Astron., 38, 29
 Kubo H., Takahashi T., Madejski G., Tashiro M., Makino F.,
 Inoue S., Takahara F., 1998, ApJ, 504, 693
 Lamer G., Brunner H., Staubert R., 1996, A&A, 311, 384
 Lin Y. C. et al., 1999, ApJ, 525, 191
 Lucas R., Liszt H. S., 1993, A&A, 276, L33
 Mineo T. et al., 2000, A&A, 359, 471
 Morrison R., McCammon D., 1983, ApJ, 270, 119
 Padovani P., Giommi P., 1995, ApJ, 444, 567
 Padovani P., Giommi P., 1996, MNRAS, 279, 526
 Parmar A. et al., 1997, A&AS, 122, 309.
 Perlman E. S., Madejski G., Stocke J. T., Rector T. A., 1999,
 ApJ, 523, L11
 Pian E. et al., 1998, ApJ, 492, L17
 Sambruna R., Maraschi L., Urry C. M., 1996, ApJ, 463, 444
 Sambruna R., Ghisellini G., Hooper E., Kollgaard R. I., Pesce J.
 E., Urry C. M., 1999, ApJ, 515, 140
 Spada M., Lazzati D., Ghisellini G., Celotti A., 2001, MNRAS,
 in press (astro-ph/0103424)
 Stickel M., Padovani P., Urry C. M., Fried J. W., Kühr H., 1991,
 ApJ, 374, 431
 Tagliaferri G. et al., 2000, A&A, 354, 431
 Tagliaferri G. et al., 2001, A&A, 368, 38
 Tanihata C., et al., 2000, ApJ, 543, 124
 Tapia S., Craine E. R., Johnson K., 1976, ApJ, 203, 291
 Tavecchio F., Maraschi L., Ghisellini G., 1998, ApJ, 509, 608
 Urry C. M., Padovani, P., 1995, PASP, 107, 803
 Urry C. M., Sambruna R. M., Worrall D. M., Kollgaard R. I.,
 Feigelson E. D., Perlman E. S., Stocke J. T., 1996, ApJ, 463,
 424
 White R. L., Giommi P., Angelini L., 1995,
<http://lheawww.gsfc.nasa.gov/users/white/wgacat/wgacat.html>
 Wolter A. et al., 1998, A&A, 335, 899